

MET O 11 TECHNICAL NOTE NO. 241

BARRIER EFFECTS IN FINE MESH MODELS

by

M.J.P. CULLEN and G.J. SHUTTS
Meteorological Office, Bracknell, U.K.

Met O 11 (Forecasting Research)
Meteorological Office
London Road
Bracknell
Berkshire RG12 2SZ
ENGLAND

SEPTEMBER 1986

This paper has been submitted to the proceedings of the ECMWF Seminar on Orography held in September 1986.

NB: This paper has not been published. Permission to quote from it must be obtained from the Assistant-Director of the Forecasting Research Branch of the Meteorological Office.

BARRIER EFFECTS IN FINE MESH MODELS

M.J.P. Cullen and G.J. Shutts
Meteorological Office, Bracknell, U.K.

Summary: Semi-geostrophic solutions for flow over a long mountain barrier are presented. They exhibit upstream blocking, a "weir" effect with a rapid downslope wind, a Föhn effect and pressure drag. The solutions agree qualitatively with many observations. They are difficult to represent accurately in fine mesh primitive equation models which tend to exhibit an excessive mountain wave response.

1. INTRODUCTION

This paper is concerned with accurate simulation by forecast models of flows over orography of a large enough scale for geostrophic control to be important and for the mountain shape to be reasonably represented by grid-point values. We use semi-geostrophic theory to increase our theoretical understanding of such flows and then relate this understanding to the design of forecast models.

The first sections of the paper present an extension of conventional semi-geostrophic theory. This theory has been used to derive analytic solutions for two dimensional flow over orography, for instance by Bannon (1984) and Pierrehumbert (1985). These solutions predict infinite ageostrophic velocities at the ridge crest when the mountain reaches a certain height. This typically happens for a height of fL/N , where N is the Brunt-Vaisala frequency, L the half width and f the Coriolis parameter. It is then usual to assume that the theory has broken down and is of no further use. Cullen (1983) proposed that, for frontal

flows, the Lagrangian form of semi-geostrophic theory still gives useful information even when there is a local breakdown of the solution. Cullen, Chynoweth and Purser (1986) make the same proposal for orographic flows. They showed that solutions obtained this way contain mountain drag, rapid downslope winds and a Föhn effect. We discuss the properties and physical validity of these extended solutions in sections 2 to 5 of this paper. The justification is less obvious than it is for fronts. While it is reasonable to argue that Lagrangian equations do not see a frontal discontinuity because the front marks an air mass boundary; it is not so reasonable to say that Lagrangian equations do not see a mountain if there is any cross mountain flow. If, however, the flow is blocked upstream of the crest for a distance of order NH/f , air above the mountain crest flows over undisturbed and air below it is deflected around the barrier; then it can be argued that no air actually undergoes a large acceleration which would invalidate semi-geostrophic theory. In practice some air does rise over the crest, and the validity of the solution depends on how much this happens.

The latter sections then discuss implications for forecast models. Two areas are examined. There is evidence that standard fine mesh primitive equation models do not produce sufficient flow separation round the Alps, but produce mountain wave activity on the scale of the whole Alpine ridge instead. The model evidently sees nothing wrong with a quasi-steady wave solution on this scale, such solutions can be produced by two dimensional finite difference models. It does not converge to an alternative quasi-steady separated solution presumably because of the near discontinuity then required in the vertical.

The second aspect to be examined is the accuracy of sigma coordinates. A severe test of this is to model a "semi-geostrophic" flow over an

equatorial ridge. The correct solution of the equations for this case gives indefinite blocking of the flow below the mountain top, and undisturbed horizontal flow above. While this is not an adequate model of real equatorial flow, it provides an extreme case to test a sigma coordinate formulation. It performs better than might be expected; suggesting that it should perform reasonably well on more realistic flows.

2. LAGRANGIAN SEMIGEOSTROPHIC THEORY

We set out this theory in its simplest form using the ζ coordinate which is a function of pressure, introduced by Hoskins and Bretherton (1972) and the form of Boussinesq approximation employed by them. Assume also that the Coriolis parameter is a constant. Then the equations take the form

$$\frac{Du_\zeta}{Dt} + f(v_\zeta - v) = 0 \quad (2.1)$$

$$\frac{Dv_\zeta}{Dt} - f(u_\zeta - u) = 0 \quad (2.2)$$

$$\frac{D\theta}{Dt} = 0 \quad (2.3)$$

$$\frac{D\alpha}{Dt} = 0 \quad (2.4)$$

$$\frac{D}{Dt} \equiv \frac{\partial}{\partial t} + u \frac{\partial}{\partial x} + v \frac{\partial}{\partial y} + w \frac{\partial}{\partial \zeta} \quad (2.5)$$

$$(f v_\zeta, -f u_\zeta, \delta \theta / \delta_\zeta) = \left(\frac{\partial \phi}{\partial x}, \frac{\partial \phi}{\partial y}, \frac{\partial \phi}{\partial \zeta} \right) \quad (2.6)$$

$$w = 0 \text{ at } \zeta = h(x, y), H \quad (2.7)$$

The Boussinesq approximation is contained in equation (2.4) where α is the specific volume of the fluid in (x, y, ζ) . Equation (2.4) would be exact if the vertical coordinate were pressure. -- The lower boundary condition has been simplified to specify it at a fixed value of ζ rather than of physical height. The rest of the notation is standard, following Hoskins and Bretherton. θ_0 is a reference value of potential temperature.

Equations (2.1) to (2.7) define (u, v, w) implicitly.

They can be solved analytically using the geostrophic coordinate transformation, e.g. Blumen (1981), Bannon (1984), Pierrehumbert (1985). Solutions can also be obtained by conformal mapping techniques, Gill (1981).

This method clearly gives unphysical results when a discontinuity forms since the solution is multivalued when transformed back to physical space. In the case of mountain flows, the breakdown is manifested as a singularity in the transformation back from a streamfunction coordinate to the physical coordinates (Pierrehumbert, 1985).

Cullen and Purser (1984) proved that the Lagrangian equations (2.1) to (2.7) can be solved as they stand. The solution is found by treating \underline{u} as a volume preserving rearrangement of the fluid. Values of u_g , v_g and θ are predicted for each fluid element by solving (2.1) to (2.3) along trajectories. Absolute momentum quantities

$$\begin{aligned} M &= v_g + f x \\ N &= -u_g + f y \end{aligned} \tag{2.8}$$

are then calculated. The dependence of (2.1) to (2.3) on \underline{u} can now be characterised as a rearrangement of fluid elements conserving M, N and θ : since the Coriolis terms are accounted for by the terms in x and y in (2.8). The rearrangement is volume preserving because of (2.4). It can then be proved that there is a unique way to arrange the fluid in physical space so that the geostrophic and hydrostatic relations (2.6) are satisfied, with M, N and θ equal to their known values on each fluid element; and so that the fluid is statically, inertially and symmetrically stable.

Cullen et al. (1986) then proved that this rearrangement can be characterised as an energy minimisation, so that the solution minimises

$$\int \frac{1}{2} (u_g^2 + v_g^2) - g\theta_g / \theta_0 \, dV$$

with respect to fluid rearrangements conserving M, N and θ . This characterisation also applies when the Coriolis parameter is allowed to vary and the Boussinesq approximation is not made, Shutts and Cullen (1986).

When there are mountains present the rearrangement is not unique. This is because air trapped in mountain valleys can be exchanged independently of the rest of the dynamics. There is still, however, a solution which

minimises the global energy. Extra information must be used to construct solutions in this case.

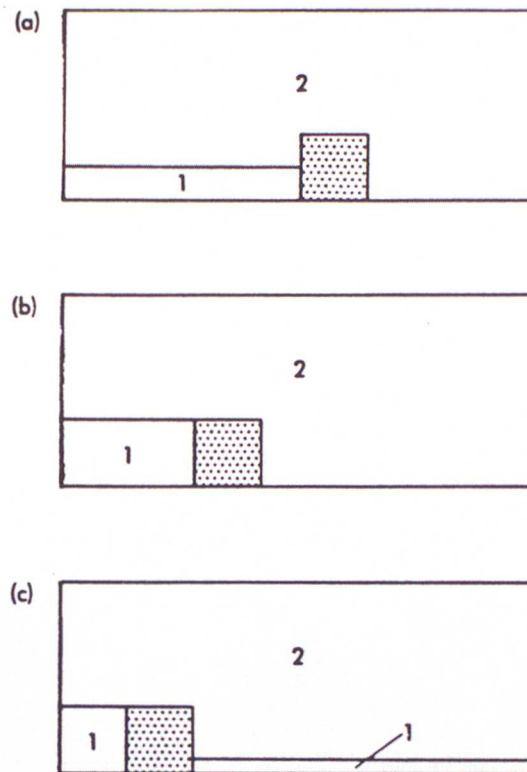


Figure 1. Two fluid model of upstream blocking without rotation.

The most physically plausible method of constructing a solution is shown in Fig. 1. For simplicity, we set the Coriolis parameter to zero so that all interfaces between fluid of different densities have to be flat. The atmosphere is represented as two fluids, with fluid 1 denser than fluid 2. A mountain barrier is then "translated" across the region, which has rigid lateral boundaries. The initial data is specified as shown in Fig. 1(a). There is a pressure difference across the barrier, but equation (2.6) is still satisfied because there are no pressure gradients within the fluid. However, any other arrangement of the fluid with a horizontal interface would also be a possible solution.

As the barrier is translated, we state that there is no flow of fluid 1 across it until the interface reaches the top. After this point, Fig. 1(b), the barrier acts as a "weir". This simple physical prescription obviously provides a unique solution to the problem as an initial-value problem.

The energy in the solution increases continuously from the configuration in Fig. 1(a) to that in Fig. 1(b). It then decreases again. A graph is shown in Fig. 2.

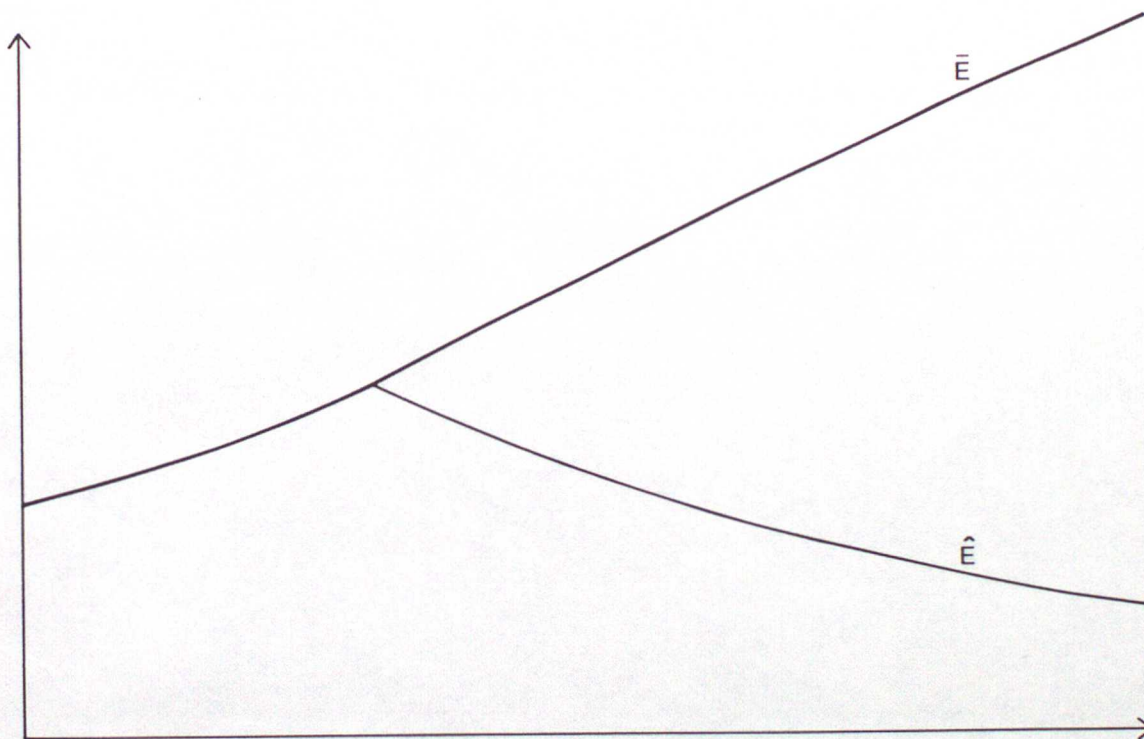


Fig. 2 Graph of work done by the drag force (\bar{E}) and the model energy (\hat{E}) during the passage of air over a barrier.

The initial rate of increase of energy is equal to the work done against the pressure gradient in moving the barrier from right to left. The subsequent decrease occurs because the energy which would appear as kinetic energy of flow over the barrier and then as waves and turbulence downstream has been deleted from the problem; providing an extremely crude parametrization of turbulent dissipation.

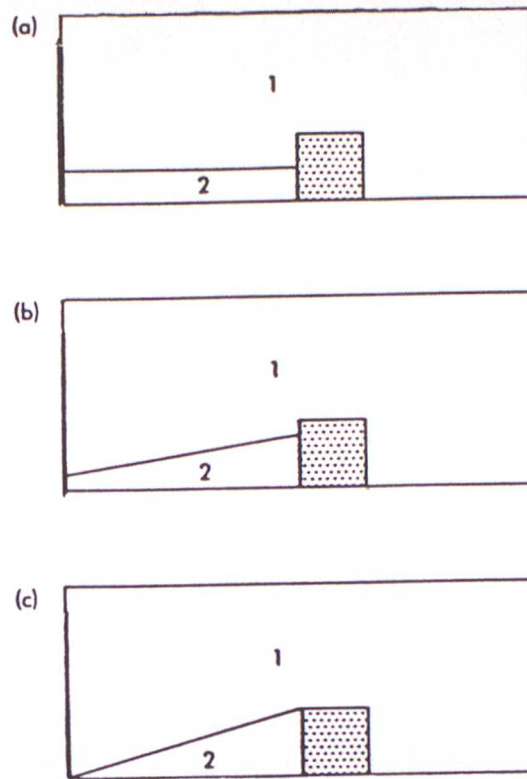


Figure 3. Upstream blocking of air in the presence of rotation.

When rotation is present the same principles are used (Fig. 3). In the initial state we assume that there is no geostrophic wind and that the diagram represents an (x, y) cross-section; this time unbounded laterally. A geostrophic cross mountain wind U is switched on, with associated pressure gradient

$$\frac{\partial \phi}{\partial y} = -fU \quad (2.9)$$

Equation (2.2) becomes

$$\frac{\partial M}{\partial t} \equiv \frac{D}{Dt}(v_y + f x) = fU \quad (2.10)$$

The slope of the interface between fluids 1 and 2 must satisfy thermal wind balance, and so is given by Margules formula :

$$\text{Slope} = \frac{f\theta_c [\nu]}{\delta [\theta]} = \frac{f\theta_c [M]}{\delta [\theta]} \quad (2.11)$$

where the square brackets indicate the difference across the interface.

Fluid 2 is blocked by the mountain in Fig. 3(a). It cannot therefore respond to the pressure gradient by increasing its value of x and therefore

increases its value of v_y . In fluid 1 there can be translation to the right at speed U so that v_y can remain zero. Thus a gradient of v_y is set up across the interface, causing it to slope (Fig. 3(b)). Eventually the interface reaches the top (Fig. 3(c)) releasing the trapped air as if over a weir. During this period a positive value of v_y will have developed according to equation (2.10). This is in agreement with observations of barrier winds, e.g. Parish (1982). The total energy in the cross section increases because it can draw on the reservoir of energy implied by the basic state pressure gradient. After fluid 2 reaches the top of the barrier the energy starts to decrease again because of the implied dissipation of the transient unbalanced cross mountain wind.

In a three dimensional flow with a barrier of finite length, it is clear that the solution in Fig. 3 will tend to produce flow around the barrier, fed by the flow along it upstream. This is frequently observed in the Alpine region, e.g. Buzzi and Tibaldi (1978).

3. EXAMPLES OF LAGRANGIAN SOLUTIONS FOR SIMPLE DATA

The solutions of equations (2.1) to (2.7) described in the previous section can be illustrated by calculating them explicitly for piecewise constant data. The calculation is easiest performed in the configuration shown in Fig. 1; using a container with rigid boundaries; and translating the mountain through it. The initial data is defined as the finite fluid elements shown in Fig. 4(a). Each element has a constant value of θ and M . The slope of inter-element boundaries is determined by Margules' formula (3.11). Elements 1 to 3 represent stratospheric air. Elements 4 to 10, 11 to 17, 18 to 24, 25 to 32 and 33 to 37 have the same values of potential temperature. The total length of the cross-section is 1000 km, with the mountain represented by a rectangular block 100 km wide and 2 km high. The mountain is translated at a uniform speed of 10 m s^{-1} . The

configuration is shown after 6 hours in Fig. 4(b) and 12 hours in Fig. 4(c).

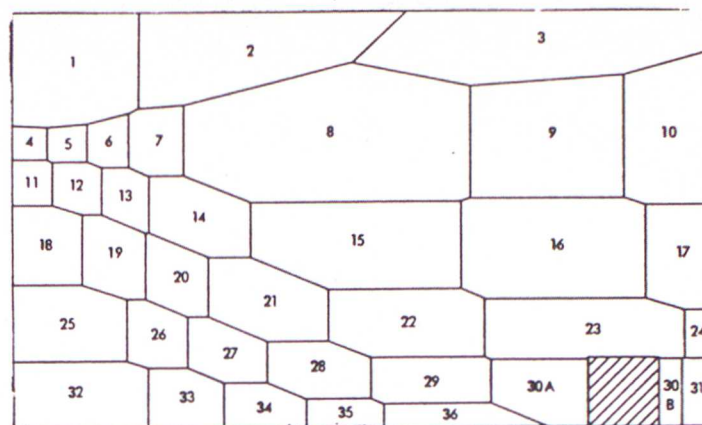


Fig. 4(a) Initial data

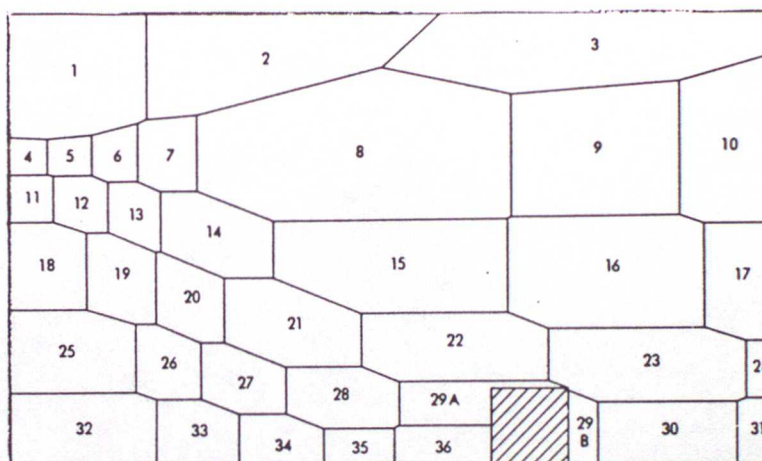


Fig. 4(b) After 6 hours

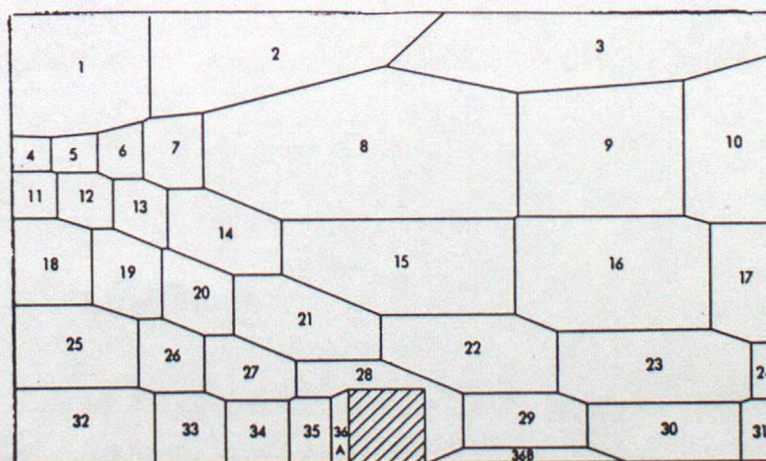


Fig. 4(c) After 12 hours

Figure 4 Flow of stratified rotating fluid over barrier.

After 6 hours, element 30 has completely crossed the barrier and element 36 is blocked behind it. There is now a drag because element 36 is denser than element 29. Element 29 is flowing across as if over a weir, element 23 has descended on the lee side giving a Föhn effect. After 12 hours element 36 has started flowing across the mountain, while element 28 has descended almost to the surface on the lee side. The drag at this time amounts to 8 pascals. Element 28 has descended by about 1 km to the lee of the barrier, implying a 10°C adiabatic warming.

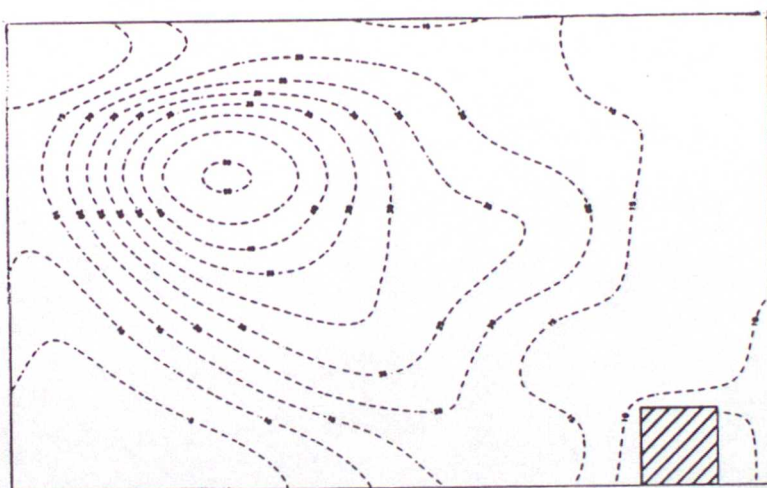


Fig. 5(a) Initial data

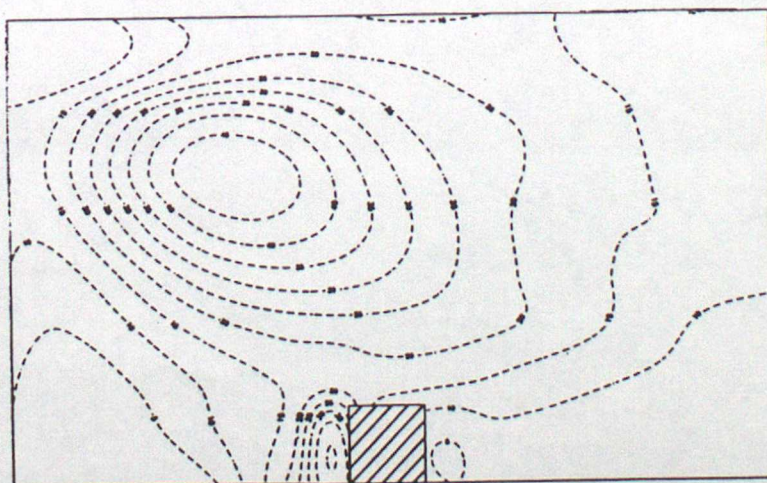


Fig. 5(b) 12 hours later

Figure 5 Plots of velocity parallel to ridge.

The along-ridge component of geostrophic wind corresponding to these solutions is shown in Fig. 5. Fig. 5(a) shows the initial data and Fig. 5(b) the solution 12 hours later. A very strong jet reaching 40 m s^{-1} is generated ahead of the barrier, with little effect at upper levels. This rather excessive value arises from the idealised two dimensional nature of the problem. The effect on the cross mountain wind is illustrated in Fig. 6. There is marked deceleration of the flow below the mountain top, with a 2 m s^{-1} deceleration extending 200 km upstream.

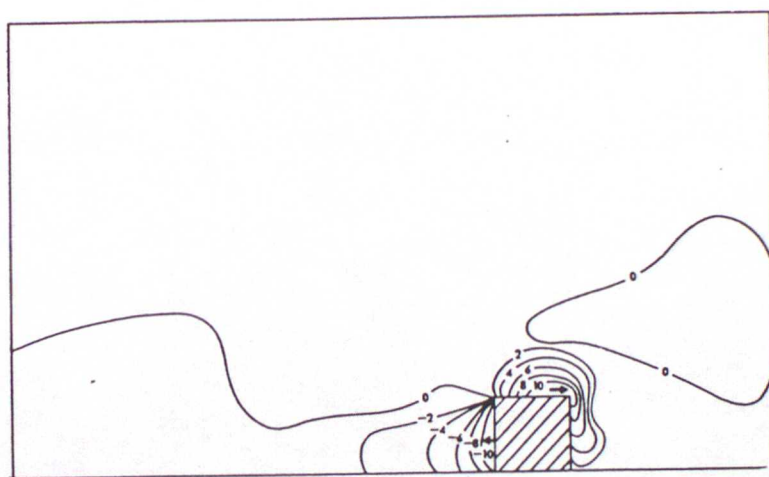


Figure 6. Horizontal cross mountain wind component after 6 hours.

A rapid acceleration of the flow in a shallow layer over the mountain top is shown which is not, however, properly described by this method. This solution is described more fully in Cullen, Chynoweth and Purser (1986).

The next experiment uses a smooth mountain profile and a two-fluid system. This can be described using much higher horizontal resolution, allowing a more realistic representation of the flow. The results are shown in Fig. 7, using 39 elements to represent the interface. The mountain has a height of 2 km and a half width of 50 km. The temperature difference across the interface is 5°K . Fig. 7 also shows the profile of v_y in the cold air, it is zero in the warm air. The diagrams show the configuration at approximately 12 hour intervals, assuming a cross mountain

flow of 5 m s^{-1} . Initially the cold air is trapped against the mountain with a southerly wind at the warm front upstream.

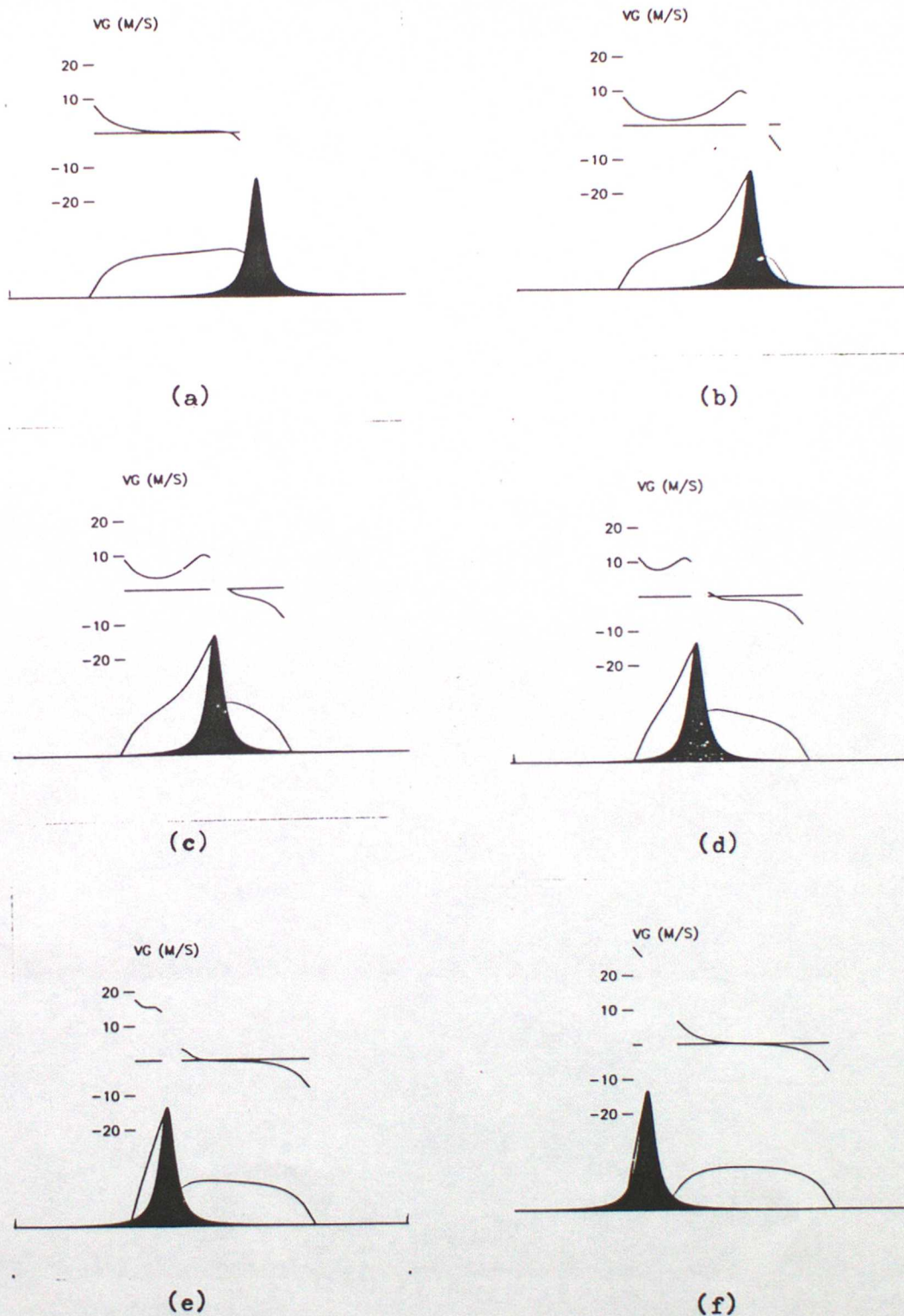


Figure 7. A sequence of model states for flow over a bell shaped mountain at intervals of $4 \times 10^4 \text{ s}$. Element boundaries are not indicated. Graphs of V_g corresponding to the fluid below are inset.

The air rises to the top of the mountain, and the first air to cross falls rapidly to the foot of the lee slope. Conservation of M results in it acquiring a northerly wind component, while a southerly jet is developing in the trapped air to windward. At later times the dome of cold air on the lee side simultaneously extends further up the mountain and further downstream. However, at all times the depth of cold air is greater on the windward side than the lee side, implying a pressure force on the mountain. As the supply of cold air crossing the mountain diminishes, so it becomes more difficult to support the cold air in its passage. A steep interface slope is needed implying a strong southerly jet, about 20 ms^{-1} , along the ridge. Finally, when all the air has crossed the mountain, the cold air dome has the same shape as before it encountered the mountain. However, work has been done by the basic state pressure gradient parallel to the ridge with a considerable net flow of air down the pressure gradient. This solution is described in more detail by Shutts (1986).

This type of solution can be calculated analytically in the special case of a steady flow across a ridge with the interface between the two fluids asymptoting to a height h_0 . The configuration is illustrated in Fig. 8.

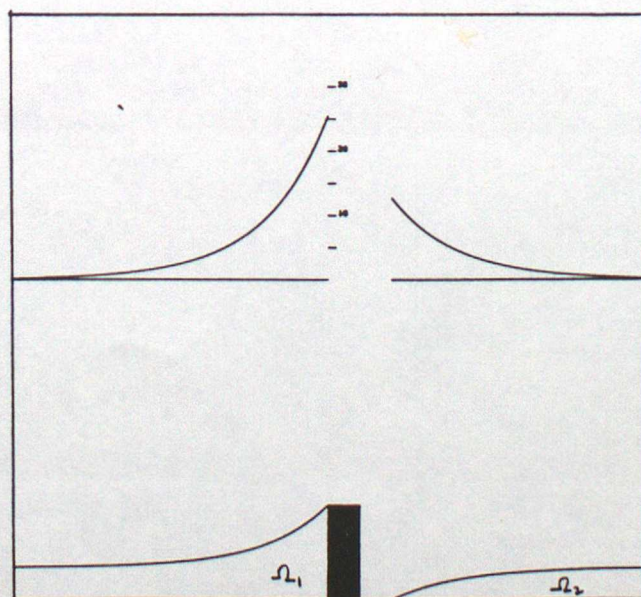


Figure 8. Steady solution for two fluid flow over a bell shaped mountain. A graph of V_g for the lower fluid is inset.

If the interface has height $h(x)$, then the geostrophic wind parallel to the ridge in the lower fluid is given by

$$v_g = \frac{g \Delta \theta}{f \theta_0} \frac{\partial h}{\partial x} \quad (3.1)$$

and the potential vorticity of the lower fluid by

$$q = \left\{ f + g \Delta \theta (\theta_0 f)^{-1} \frac{\partial^2 h}{\partial x^2} \right\} / h \quad (3.2)$$

If the solution is to be steady, conservation of q implies that q must be uniform in x and equal to f/h_0 . This implies

$$h f / h_0 = f + g \Delta \theta (\theta_0 f)^{-1} \frac{\partial^2 h}{\partial x^2} \quad (3.3)$$

The upstream configuration, with cold air just reaching the top of the barrier of height H , is given by

$$h = h_0 + (H - h_0) \exp(f x / \sqrt{g \Delta \theta h_0 \theta_0^{-1}}) \quad (3.4)$$

To find the downstream configuration, we use the equality of the values of M at the mountain top and in the rear edge of the downstream cold air.

M is easily calculated from (3.1) and we find that the downstream solution is

$$h(x) = h_0 - \exp(H - h_0 - (f x / \sqrt{g \Delta \theta h_0 \theta_0^{-1}})) \quad (3.5)$$

with x_0 satisfying

$$h_0 = \exp(H - h_0 - f x_0 / \sqrt{g \Delta \theta h_0 \theta_0^{-1}}) \quad (3.6)$$

In this configuration, the pressure drag on the mountain is equal to

$$\int_0^H \delta p \, dz$$

at $x = 0$. Using continuity of the pressure at $z = H$, $x = 0$ gives

$$\begin{aligned} \int_0^H \rho_0 g \Delta \theta (H - z) \, dz \\ = \frac{1}{2} \rho_0 g \Delta \theta H^2 \end{aligned} \quad (3.7)$$

The rate of working of the geostrophic pressure field is given by

$$\int \Omega_1 v_g \frac{d}{dz} (\delta p) \, dx \, dz + \int \Omega_2 v_g \frac{d}{dz} (\delta p) \, dx \, dz \quad (3.8)$$

Since $f u_g = \frac{1}{\rho_0} \frac{d}{dz} (\delta p)$

$$\begin{aligned} \text{this is equal to } & f \rho_0 u_g \left[\int_{-\infty}^0 f^{-1} g \Delta \theta h \frac{\partial h}{\partial x} \, dx + \int_{x_0}^{\infty} f^{-1} g \Delta \theta h \frac{\partial h}{\partial x} \, dx \right] \\ & = \rho_0 g u_g \Delta \theta \left[\left[\frac{1}{2} h^2 \right]_{-\infty}^0 + \left[\frac{1}{2} h^2 \right]_{x_0}^{\infty} \right] \\ & = \frac{1}{2} \rho_0 g u_g \Delta \theta H^2 \end{aligned} \quad (3.9)$$

which is the rate of work of the mountain drag (3.7).

4. FINITE DIFFERENCE SOLUTIONS FOR SEMI-GEOSTROPHIC FLOW OVER A BARRIER

In this section we illustrate solutions of equations (2.1) to (2.7) obtained by finite difference methods. The solution shown was for a two dimensional version of the problem written in sigma coordinates and standard notation :

$$\frac{D}{Dt} (v_g + f x) = f U \quad (4.1)$$

$$\frac{\partial \theta}{\partial t} = 0 \quad (4.2)$$

$$\frac{D}{Dt} \equiv \frac{\partial}{\partial t} + u \frac{\partial}{\partial x} + \sigma \frac{\partial}{\partial \sigma} \quad (4.3)$$

$$\frac{\partial p^*}{\partial t} + \frac{\partial}{\partial x} (p^* u) + \frac{\partial}{\partial \sigma} (p^* \sigma) = 0 \quad (4.4)$$

$$\frac{\partial \phi}{\partial x} + R T \frac{\partial}{\partial x} (\ln p^*) = f v_g \quad (4.5)$$

$$\frac{\partial \phi}{\partial \sigma} + \frac{R T}{\sigma} = 0 \quad (4.6)$$

$$T = \theta (p/p_0)^{\kappa}, \kappa = R/c_p \quad (4.7)$$

$$\sigma = 0 \text{ at } \sigma = 0, 1 \quad (4.8)$$

$$u = U \text{ at } x = -L, L \quad (4.9)$$

Equations (4.1) to (4.8) determine u and σ implicitly. They are approximated by second order finite differences on a staggered mesh as shown in Fig. 9. This gives a block tridiagonal system of implicit equations.

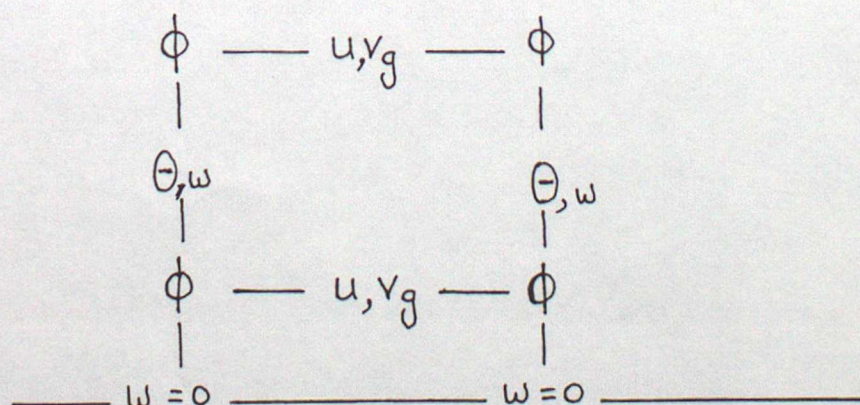


Figure 9. Arrangement of variables on the vertical cross section grid.

The method of solution is as follows :

- (a) Choose initial ρ_*, θ , with $\rho_*(-L) = \rho_*(L) = \rho_0$
- (b) Solve (4.5) and (4.6) for v_g .
- (c) Initially set $u = \rho_0 U / \rho_*$, so $\dot{\sigma} = 0$
- (d) Solve equations (4.1) and (4.2) for v_g and θ using an implicit time differencing scheme of the form

$$\theta(t + \Delta t) - \theta(t) = -\{(1-\alpha)(\underline{u} \cdot \nabla \theta)_t + \alpha(\underline{u} \cdot \nabla \theta)_{t+\Delta t}\} \quad (4.10)$$
 with $\frac{1}{2} \leq \alpha \leq 1$ (α was chosen as 0.7 in the integrations illustrated); and $\underline{u} \cdot \nabla \equiv u \frac{\partial}{\partial x} + \dot{\sigma} \frac{\partial}{\partial \sigma}$.
- (e) Calculate the residual in equation (4.5) at time $t + \Delta t$; write it as R .
- (f) Recalculate $u(t + \Delta t), \dot{\sigma}(t + \Delta t)$ to eliminate R , by solving the coupled system.

$$\Delta \theta + \Delta \underline{u} \cdot \nabla \theta + \underline{u} \cdot \nabla (\Delta \theta) = 0 \quad (4.11)$$

$$\Delta v_g + \Delta \underline{u} \cdot \nabla v_g + \underline{u} \cdot \nabla (\Delta v_g) + f \Delta u = 0 \quad (4.12)$$

$$\Delta \rho_* + \frac{\partial}{\partial x} (\rho_* \Delta u + u \Delta \rho_*) + \frac{\partial}{\partial \sigma} (\rho_* \Delta \dot{\sigma} + \dot{\sigma} \Delta \rho_*) = 0 \quad (4.13)$$

$$\Delta \dot{\sigma} = 0 \quad \text{at } \sigma = 0, 1 \quad (4.14)$$

$$\Delta u = 0 \quad \text{at } x = -L, L \quad (4.15)$$

$$\frac{\partial}{\partial x} \Delta \phi + R T \frac{\partial}{\partial x} u \Delta \rho_* + R \Delta T \frac{\partial}{\partial x} h \rho_* - f \Delta v_g = -R \quad (4.16)$$

$$\frac{\partial \Delta \phi}{\partial \sigma} + \frac{R \Delta T}{\sigma} = 0 \quad (4.17)$$

Elimination of $\Delta \dot{\sigma}$ using (4.13), $\Delta \phi$ using (4.17) and ΔT using a differentiated form of (4.7) reduces this system to a block tridiagonal system with $3N \times 3N$ blocks where the model has N levels. The unknowns are N values of Δv_g , $N-1$ values of $\Delta \theta$, 1 value of $\Delta \rho_*$ and N values of Δu for each value of x . The system can then be written in the form

$$\underline{C} \underline{w}_{x-\Delta x} + \underline{A} \underline{w}_x + \underline{B} \underline{w}_{x+\Delta x} = \underline{F} \quad (4.18)$$

where \underline{C} , \underline{A} , \underline{B} are $3N \times 3N$ matrices, \underline{w} is a $3N$ column vector and \underline{F} is a $3N$ column vector. This system can be solved by standard techniques.

Cullen and Purser (1984) prove that u and $\dot{\sigma}$ are uniquely determined by

this system in the absence of orography provided that the solution is required to be statically, inertially and symmetrically stable; so that the potential vorticity is non-negative. In the presence of a mountain ridge, Cullen et al. (1986) show that the solution is still uniquely determined as long as all fluid is required to reach the top of the ridge before passing over it. The solution contains large horizontal jumps in the position of fluid parcels, as described in section 3. This causes similar numerical difficulties to the presence of static instability in the vertical. An adjustment is therefore incorporated in the model to remove inertial instability and replace negative gradients of $(v_g + \frac{1}{2}x)$ in x with small positive ones. This acts as a parametrization of the rapid downslope wind which is in any case not realistically represented by the semi-geostrophic equations.

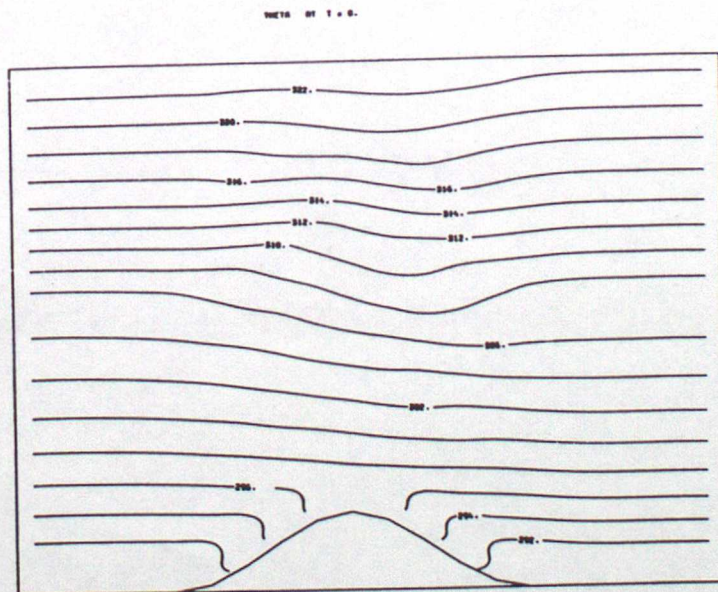


Fig. 10(a) Potential temperature.

Figure 10. Initial data for simulation of flow over ridge.

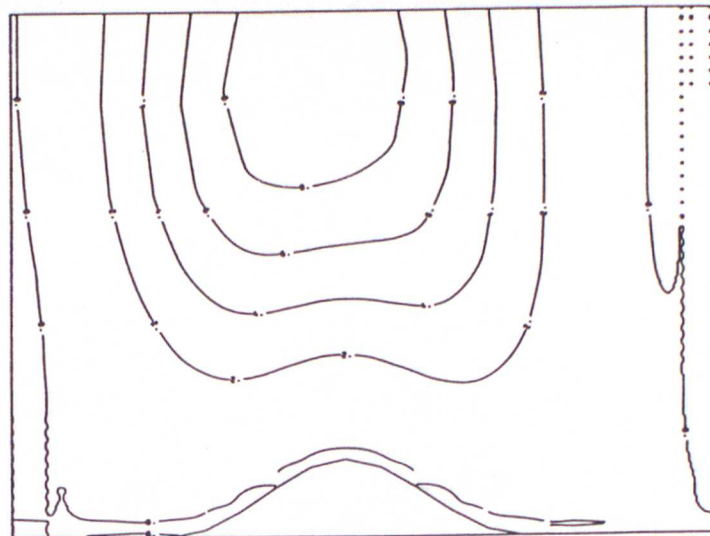


Fig. 10(b). Velocity parallel to ridge.

A solution is shown in Figs. 10 and 11. The mountain ridge is 1800 m high, the channel length 1000 km and the mountain width 200 km. The basic cross mountain flow was 10 ms^{-1} . A 20×10 grid was used. Fig. 10 shows the initial data for Θ and v_y . Fig. 11 shows the solution after 12 hours.

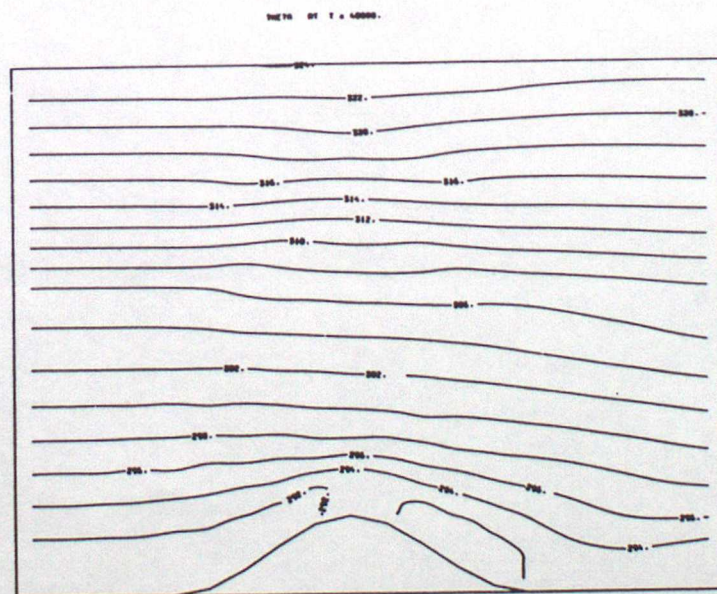


Fig. 11(a) Potential temperature.

Figure 11. Flow fields after $4 \times 10^4 \text{ s}$.

U AT T = 40000.

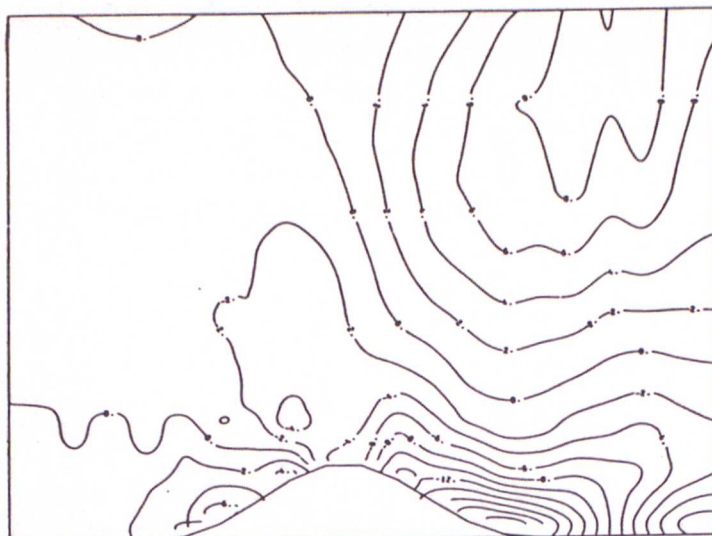


Fig. 11(b) Along ridge wind.

U AT T = 40000.

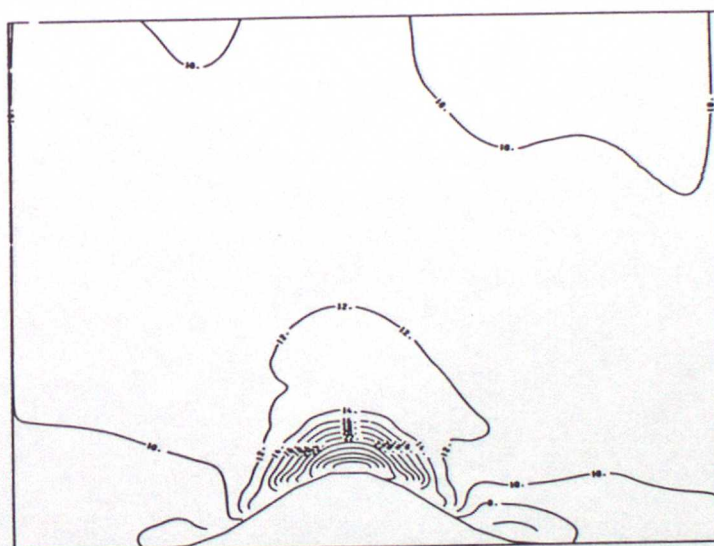


Fig. 11(c) Cross ridge
horizontal wind.

W AT T = 40000.

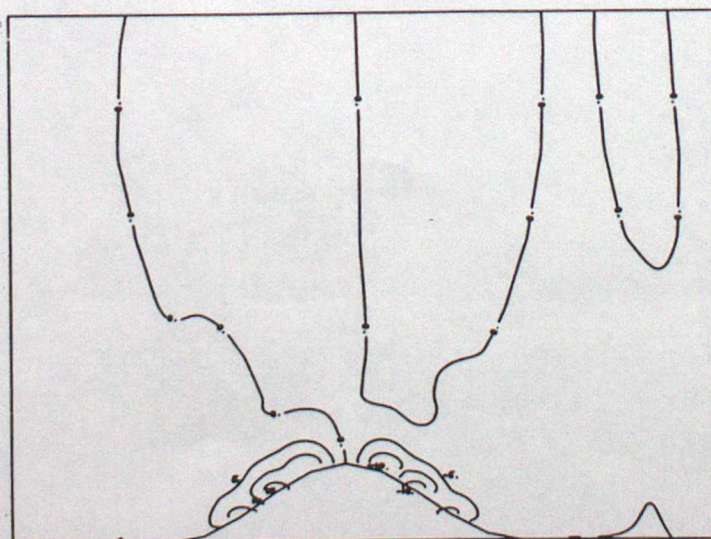


Fig. 11(d) Vertical velocity.

The θ field (Fig. 11(a)) illustrates upstream blocking with some cold air beginning to flow down the lee side. The v_g field illustrates the "start" vortex at low levels which results from the use of initial data varying smoothly across the mountain top. The u field shows the upstream blocking and very concentrated rapid flow at low levels over the top of the ridge, with little disturbance above. It does not show the downslope wind because it is represented by a parametrization. The total wind would have to be calculated by adding the mass transport implicit in the inertial adjustment. The drag on the mountain at this time was 0.47 Nm^{-2} .

This finite difference solution is not entirely satisfactory. There is considerable noise downstream which appears incorrect from the simple structure of the solutions described in section 3. It is caused by the difficulty of handling the rapid downslope current satisfactorily, even when it is parametrized.

5. PHYSICAL RELEVANCE OF SEMI-GEOSTROPHIC SOLUTIONS

The three preceding sections have described a class of highly singular separated flow solutions for flow over a barrier. If these solutions approximate real atmospheric behaviour, then it is clear that they may not be well represented in conventional forecast models. In this section we briefly make a qualitative comparison between these solutions and observations.

The existence of intense low-level jet streams running parallel to mountain ridges has been documented by Schwerdtfeger (1975) and Parish (1982), both being related to the damming of cold air. Parish found winds of $15 - 30 \text{ ms}^{-1}$ along the Sierra Nevada mountains at levels below 2.7 km, particularly in association with the approach of cold fronts. These jets were typically of 100 km horizontal extent and compare well with the semi-geostrophic solutions described here. Unfortunately, lee-side

observations were not available to confirm the existence of a weir.

Conversely, Reed (1981) and Mass and Albright (1985) describe lee-side windstorms in association with cold air dammed against the eastern side of the Cascade Mountains (Washington State, USA) though do not mention barrier jetstreams explicitly. Nevertheless, the potential temperature cross-sections they present are highly reminiscent of the cold air distribution found in the semi-geostrophic model. Cold air extends up the windward side of the Cascade mountains forming a very stable layer near the mountain ridge crest. Potentially warm air exists on the lee-side above a 'bora-like' downslope current of great intensity. There is also a hint of a cold air dome 100 km downstream of the ridge in Reed's study, though it is insufficiently resolved to justify comparison with the model. Large pressure differences across the mountain ridge were present in both cases with values up to 17mb. Many other observational studies have found large pressure forces to act on mountain ridges (e.g. Davies and Phillips, 1985 and Smith, 1978) Hoinka (1985) noted a large discrepancy between the synoptic-scale pressure force acting on the Alps ($1.6-7 \text{ Nm}^{-2}$) in a south Föhn event and the mid-tropospheric vertical momentum flux measured from an aircraft (0.3 Nm^{-2}) suggesting that much of the energy dissipation/wave radiation was taking place in the lower troposphere. The semi-geostrophic model strongly suggests that this synoptic scale drag force is predominately associated with cold air damming and local energy dissipation rather than vertically radiating gravity waves. Although in our two-dimensional model the cold air escapes over the mountain, in reality the release may also take place around mountain ridges with similar effect.

A further interesting finding from the ALPEX project is the existence of very intense wind shears at the level of the mountain tops and upstream of the Alps during orographic blocking episodes. A pronounced ($\sim 90^\circ$) veering of the wind is often observed to occur in a layer little more than

100 m deep accompanied by a marked inversion (Pierrehumbert and Wyman, 1985). These phenomena have their direct counterparts in the model since the wind speed and direction and the potential temperature are all discontinuous at the dome interface. The directional shear is particularly noticeable close to the ridge where the barrier jet (almost parallel to the ridge) gives way to the uniform geostrophic basic state current in the warm air above.

All these studies suggest that the semi-geostrophic solution is at least a useful qualitative model of blocked and separated flows. The total mass transport and drag is predicted by the model and is entirely determined by the large scale balanced flow. The details of flow across the mountain are not described and a more complete dynamical description is needed. In a forecast model, however, the resolution is not usually sufficient to justify attempting to predict any more than the quantities determined by semi-geostrophic theory.

6. IMPLICATIONS FOR FORECAST MODELS

The previous sections have shown semi-geostrophic solutions which appear to be physically important and should be predicted by forecast models. It would be natural to hope that a primitive equation model would be able to generate any solution predicted by semi-geostrophic theory, as well as other solutions. However, in integrating the primitive equations it is necessary to enforce smoothness. We will illustrate that this prevents accurate simulation of the discontinuous semi-geostrophic solutions because a smooth but unbalanced solution is found instead.

The forecast shown is from data for 12 GMT on 2 March 1984. The 500mb and PMSL charts are shown in Figs. 12(a) and 12(b). There was a strong north-westerly flow over the Alps in association with a deep vortex over the North Sea and a large trough over the eastern Mediterranean.

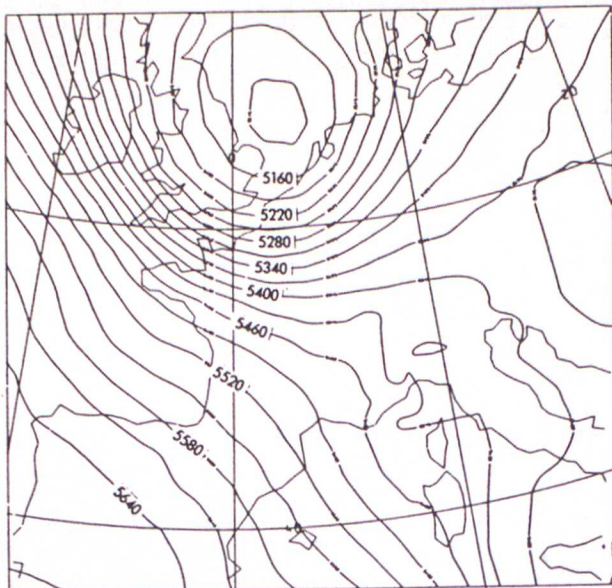


Fig. 12(a) 500 mb height.

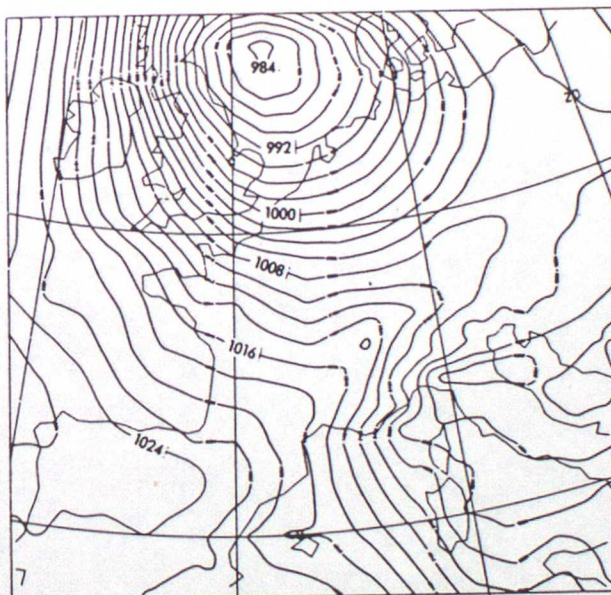


Fig. 12(b) PMSL.

Figure 12 Initial data for fine mesh integration.

18 hour forecasts are shown using a $\frac{1}{8}^{\circ} \times \frac{1}{32}^{\circ}$ grid in the Meteorological Office fine mesh model (Gilchrist and White, 1982). The orography is shown in Fig. 13. The maximum height resolved is 2500 m and the general ridge height is about 1800 m.

The forecast wind at $\sigma = 0.87$ is shown in Fig. 14. Similar results are obtained at the level below and above ($\sigma = 0.94$ and $\sigma = 0.79$). The vortex has transferred into Germany and a lee cyclone has developed over Northern Italy.

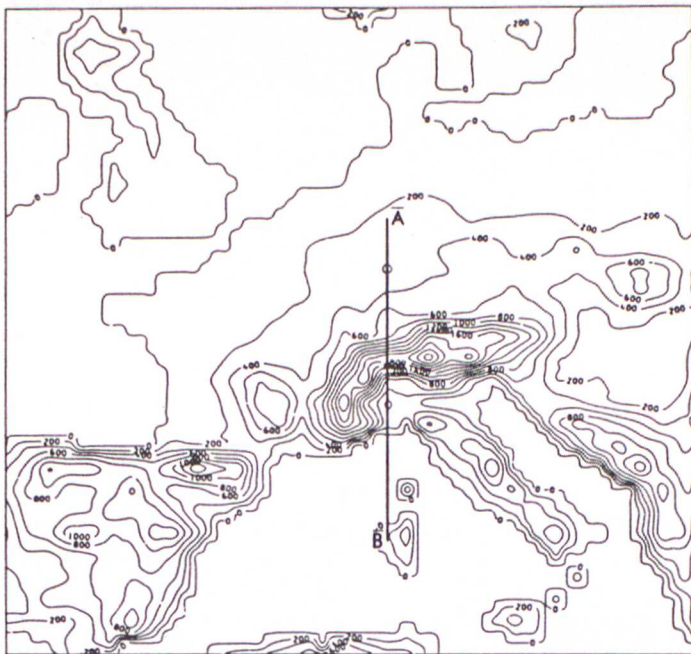


Figure 13.
Orography field for fine
mesh integration.

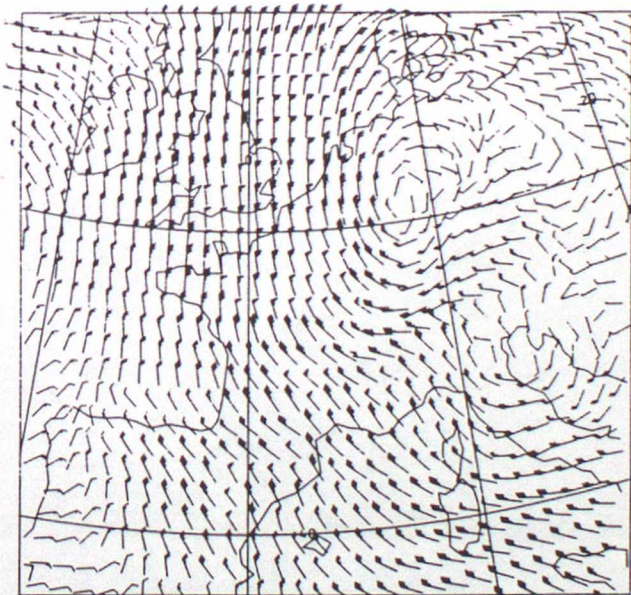


Figure 14. 18 hour forecast :
velocity field at $\sigma = 0.87$

There is no obvious sign of flow separation or distortion by the Alps at this level or the adjacent levels in the model, in particular the discontinuities in wind direction observed during ALPEX do not seem to be present.

Vertical cross sections along the line AB in Fig. 13 are shown in Fig. 15. The potential temperature cross-section (Fig. 15(a)) shows a well marked tropospheric frontal zone and potentially colder air near the

surface to the north of the Alps.

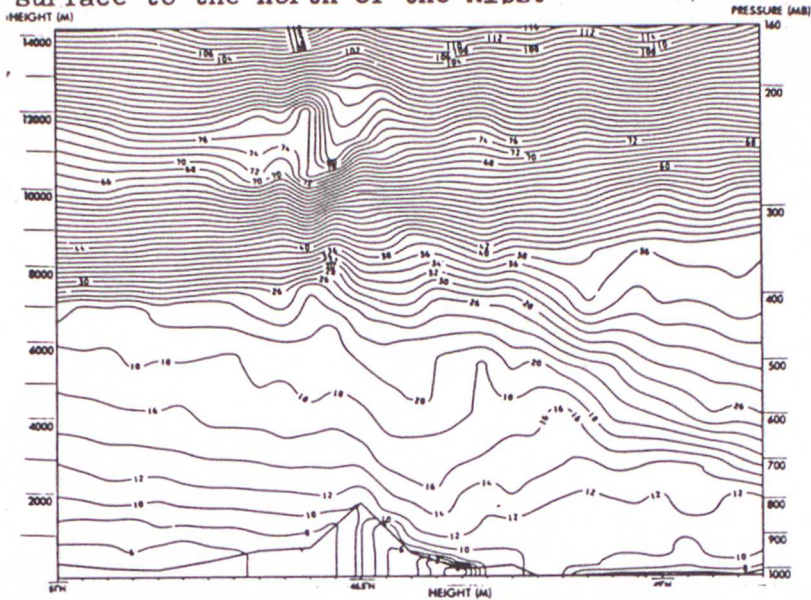


Fig. 15(a) Potential temperature.

Fig. 15(b) Transverse horizontal wind (ms^{-1}).

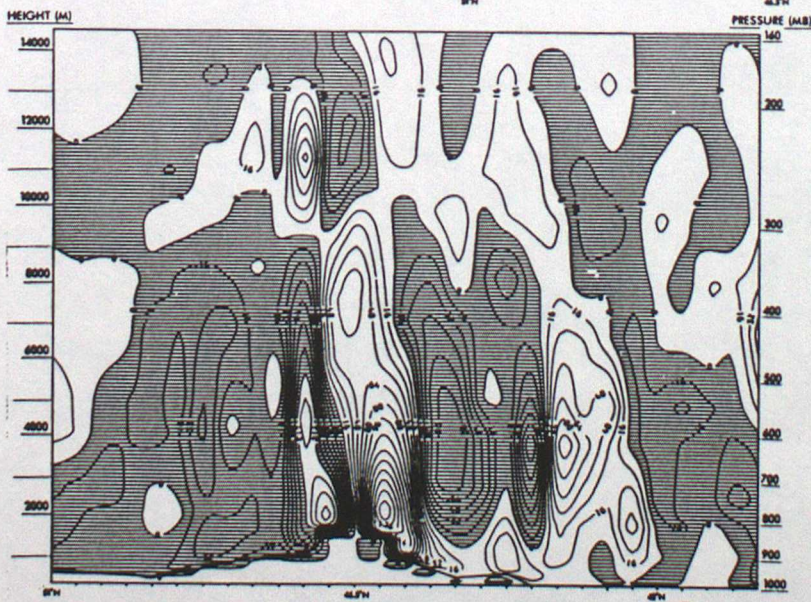
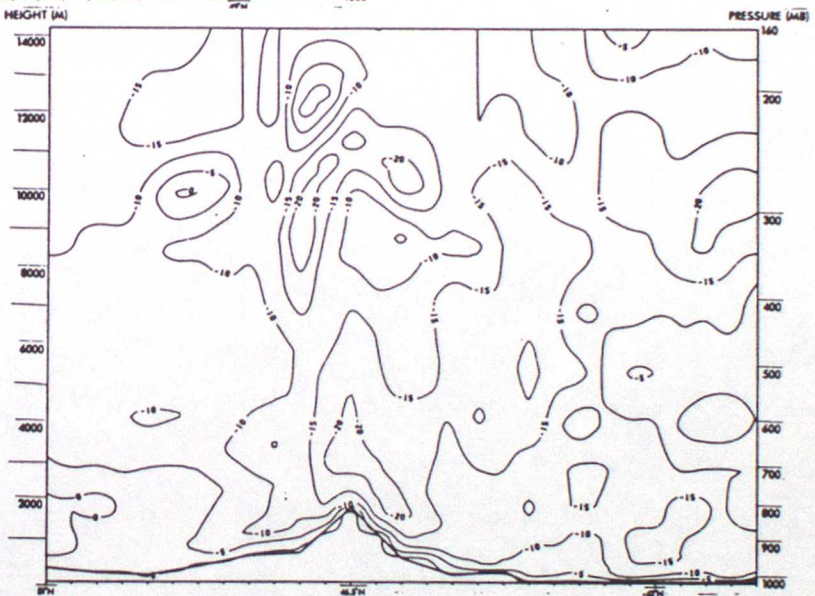


Fig. 15(c) Vertical velocity (cm s^{-1}).

Figure 15 Vertical cross-sections from 18 hour fine mesh forecast.

mountain where the value should be about 2 ms^{-1} . The isentropes should remain horizontal across the mountain. The solution reproduces the correct behaviour away from the mountain but there are local errors in the region of steepest orographic slope. This illustrates that a sigma coordinate model can represent the configuration quite accurately.

u at $t = 40000$.

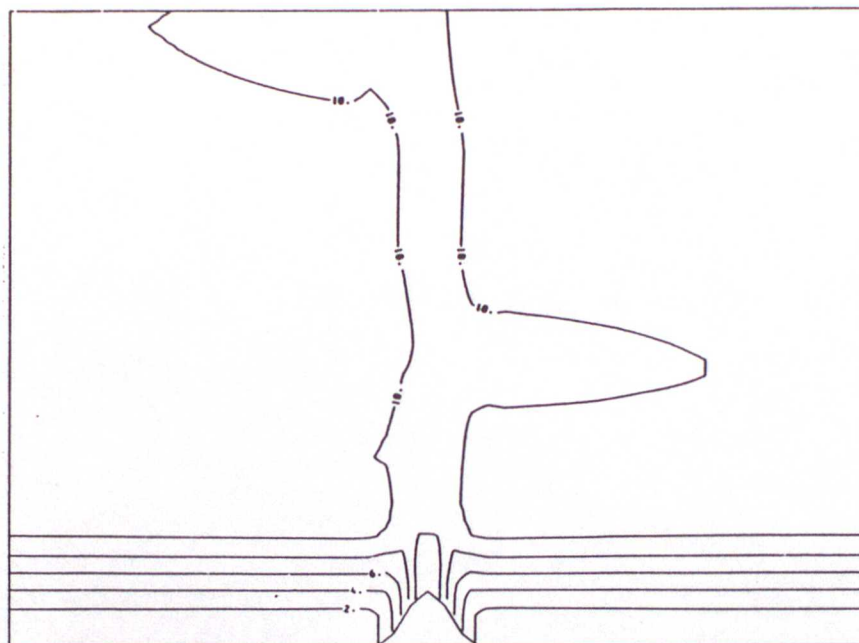


Fig. 16(a) Potential temperature.

THEIR at $t = 40000$.

Fig. 16(b) Wind perpendicular to mountain.

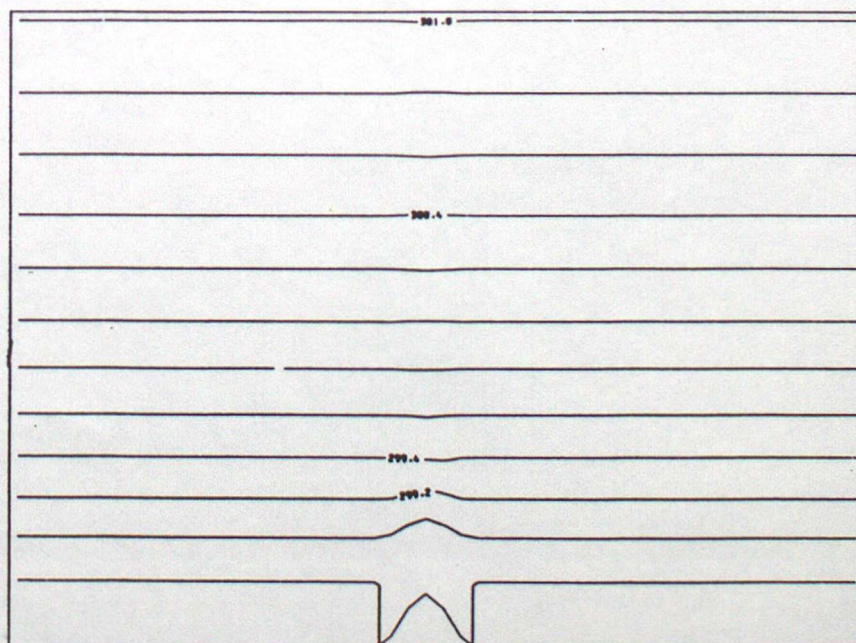


Figure 16. Finite difference solution of orographic blocking without rotation.

However, it also shows what appears to be considerable mountain wave activity. The wave slopes upstream with height and causes the isentropes to overturn in the lower stratosphere. The horizontal and vertical velocity cross-sections, Figs. 15(b) and (c), also indicate a wave. The structure of the wave and the vertical amplitude agree with observed mountain waves, Hoinka (1985), Klemp and Lilly (1978) and with the computations in the latter paper. However, their horizontal scale appears unrealistically large. While observations are not available to conclusively state that the model is behaving incorrectly, it appears to be producing a response appropriate to a smaller scale where the Coriolis effect is unimportant, instead of producing a vertically discontinuous solution of the type suggested by semi-geostrophic theory. This case is discussed at greater length by Cullen and Parrett (1986). It is not at all clear how the solution can be altered, although the wave can be smoothed out, smaller and realistic mountain waves would then be removed as well.

It is often claimed, e.g. Mesinger (1984), that the use of sigma coordinates results in spurious pressure gradients and therefore possibly spurious mountain waves. We therefore illustrate a calculation which is a severe test of sigma coordinates to estimate the size of the likely errors. The problem solved in section 4 is now repeated with the Coriolis term set to zero and periodic boundary conditions used. The absence of geostrophic balance requires all the isentropes to be horizontal and the flow to be completely blocked below the mountain top. The horizontal velocity on the lower sigma layers therefore has to jump discontinuously from zero to the free stream value of 10 m s^{-1} over the mountain. The result is shown in Fig. 16. The mountain is 800 m high and the lowest model level is about 1000 m deep. The expected solution is for a free stream velocity of 10 m s^{-1} except in the lowest layer away from the

7. DISCUSSION

This paper has presented a class of semi-geostrophic solutions for mountain flow which exhibit many realistic features. They are discontinuous in space and are thus difficult to maintain in primitive equation models. Evidence is present to suggest that a smooth unbalanced solution is obtained instead. The semi-geostrophic solution predicts large and realistic values for mountain drag which are fully predictable given the large scale balanced flow and the mountain shape, particularly the barrier height. This drag must be accurately represented in forecast models. It is not clear how well it is treated at present. The rapid downslope currents may require parametrization in primitive equation models or inertial instability could be generated. The solution thus provides a severe and important test.

We have been entirely concerned with fine mesh models where the shape of the orography is adequately represented. It is clear that the semi-geostrophic solution is critically dependent on the barrier height, so that a low resolution model which underestimates it will give a poor solution. The onset of flow separation at the breakdown point of the geostrophic coordinate transformation takes place for a critical curvature of the mountain; as discussed by Shutts (1986). If the mountain is represented too smoothly in a low resolution model then the radius of curvature will not fall to the critical value and no separation will occur. The question of parametrization of sub grid-scale orography is discussed by other papers in this volume. It is not clear whether there is any real substitute for adequate resolution of the mountain shape.

8. ACKNOWLEDGEMENTS

The computer code for the element solutions was written by Mr. S. Chynoweth. The finite difference calculations were carried out by Mr. C.A. Parrett.

9. REFERENCES

- Bannon, P.R., 1984: A semi-geostrophic model of frontogenesis over topography. *Beitr. Phys. Atmos.* 57, 393-408.
- Blumen, W., 1981: The geostrophic coordinate transformation. *J. Atmos. Sci.*, 38, 1100-1105.
- Buzzi, A. and S. Tibaldi, 1978: Cyclogenesis in the lee of the Alps: a case study. *Quart. J. Roy. Meteor. Soc.*, 104, 271-287.
- Cullen, M.J.P., 1983: Solutions to a model of a front forced by deformation. *Quart. J. Roy. Meteor. Soc.*, 109, 565-573.
- Cullen, M.J.P. S. Chynoweth and R.J. Purser., 1986: On semi-geostrophic flow over synoptic scale topography. U.K. Met. Off., Met O 11 Technical Note No 216, submitted to *Quart. J. Roy. Meteor. Soc.*
- Cullen, M.J.P. and C.A. Parrett, 1986: Mountain wave generation by models of flow over synoptic scale orography. U.K. Met. Off., Met O 11 Technical Note No 216, submitted to *Quart. J. Roy. Meteor. Soc.*
- Cullen, M.J.P. and R.J. Purser, 1984: An extended Lagrangian model of semi-geostrophic frontogenesis. *J. Atmos. Sci.*, 41, 1477-1497.
- Davies, H.C. and P.D. Phillips, 1985: Mountain drag along the Gotthard section during ALPEX. *J. Atmos. Sci.*, 42, 2093-2109.
- Gilchrist, A. and P.W. White, 1982: The development of the Meteorological Office new operational forecasting system. *Meteor. mag.*, 111, 161-179.
- Gill, A.E., 1981: Homogeneous intrusions in a rotating stratified fluid. *J. Fluid. Mech.*, 103, 275-295.
- Hoinka, K.P., 1985: Observations of the airflow over the Alps during a Foehn event. *Quart. J. Roy. Meteor. Soc.*, 111, 199-224.
- Hoskins, B.J. and F.P. Bretherton, 1972: Atmospheric frontogenesis models: mathematical formulation and solution. *J. Atmos. Sci.*, 29, 11-37.
- Klemp, J.B. and D.K. Lilly, 1978: Numerical simulation of hydrostatic mountain waves. *J. Atmos. Sci.*, 35, 78-107.
- Mass, C.F. and M.D. Albright, 1985: A severe windstorm in the lee of the Cascade mountains of Washington State. *Mon. Weath. Rev.*, 113, 1261-1281.
- Mesinger, F., 1984: Vertical finite-difference representation in weather prediction models. GARP special report no 43, I-33-49.
- Parish, T., 1982: Barrier winds along the Sierra Nevada mountains. *J. Appl. Met.*, 21, 925-930.
- Pierrehumbert, R.T., 1985: Stratified semi-geostrophic flow over two-dimensional topography in an unbounded atmosphere. *J. Atmos. Sci.*, 42, 523-526.
- Pierrehumbert, R.T. and B. Wyman, 1985: Upstream effects of mesoscale mountains. *J. Atmos. Sci.*, 42, 977-1003.

Reed, R.J., 1981: A case study of a bora-like windstorm in western Washington. Mon. Weath. Rev., 109 , 2383-2393.

Schwerdtfeger, W., 1975: The effect of the Antarctic peninsula on the temperature regime of the Weddell Sea. Mon. Weath. Rev., 103 , 45-51.

Smith, R.B., 1978: A measurement of mountain drag. J. Atmos. Sci., 35 , 1644-1654.

Shutts, G.J., 1986: The semi-geostrophic weir. U.K. Met. Off., Met O 11 Technical Note No 237.

Shutts, G.J. and M.J.P. Cullen, 1986: Parcel stability and its relation to semi-geostrophic theory. U.K. Met. Off., Met O 11 Technical Note No 232, submitted to J. Atmos. Sci.